Geometric Accuracy Comparison of Shorelines Derived from Multitemporal Sentinel-2A Imagery with Various Image Spectral Transformations (Case Study: Marine Deposition Coasts in Bantul Regency, Yogyakarta, Indonesia)

Wicaksono, A.,[1,2] Khakhim, N.,[1] Pratama, D. N. D.,[1] Musthofa, A.[3] and Lazuardi, W.[1,2]
[1]Departement of Geographic Information Science, Faculty of Geography, Universitas Gadjah Mada, Yogyakarta, Indonesia.
[2]Master Program in Planning and Management of Coastal and Watershed, Faculty of Geography, Universitas Gadjah Mada, Yogyakarta, Indonesia.
[3]Departement of Development Geography, Faculty of Geography, Universitas Gadjah Mada, Yogyakarta, Indonesia, E-mail: nurulk@ugm.ac.id

Abstract
Shoreline extraction from Landsat imagery is limited to 30m spatial resolution. The presence of Sentinel-2A imagery opens up opportunities for shoreline extraction for larger-scale mapping; thus, it is necessary to investigate the capability and limitations of various spectral transformations in mapping multitemporal shoreline positions. This study presents a methodology for processing Sentinel-2A imagery and methods for semi-automatic shoreline extraction. Experiments were carried out on marine deposition coasts as the coastal physical typology developing on most Indonesian coasts. The 20m Sentinel-2A imagery data acquired in 2015 until 2020 were compared with several spectral transformation methods: Automated Water Extraction Index Non-Shadow (AWEInsh), Automated Water Extraction Index Shadow (AWEIsh), Modified Normalized Difference Water Index (MNDWI), Normalized Difference Water Index (NDWI), Band Ratio (B3/B11), and Single Band (B11). The use of multitemporal imagery aims to test image and method consistencies in extracting shorelines accurately. The image acquisition time for each year was selected by taking into account cloud cover, land-sea contrast boundary (delimited with Otsu's image thresholding algorithm), and data availability. The accuracy was assessed with small-format aerial photographs of 0.3m spatial resolution. The results indicated that MNDWI produced shorelines with RMSE ranging from 32 to 64 m, which meets the class-3 standard for 1: 50,000 scale maps per the Indonesian Geospatial Information Agency's (Badan Informasi Geospasial, BIG) Regulation Number 6 of 2018. Therefore, 20m Sentinel-2A can be used as a data source in rapid shoreline extraction. Several factors contributing to RMSE that is 3 to 6 times greater than the spatial resolution of Sentinel-2A images include cloud cover, mixed pixels, foam, and tidal bias, creating data uncertainty values ranging from 28 to 45 m.

1. Introduction

Shorelines change in a short or slow time depending on the balance between nearshore sediment motions by waves and currents (Triadmojo, 2008), topography (Sinaga and Susiati, 2007), coastal material, tides, and wind (Dulbahri, 1983). Each map can use shorelines with different sea-level positions depending on the purpose of the mapping (Wicaksono and Wicaksono, 2019b). Shoreline data quality is observable from positional, temporal, and attribute accuracies. Positional accuracy assessment is necessary for evaluating the quality of spatial datasets (Girres and Touga, 2010) as it determines how close the positions of discrete objects or features are to their actual locations on the ground (Congalton and Green, 2008). A high water line (HWL) is used as a shoreline indicator because it appears as the contrast boundary between wet and dry coastal sediments from the last maximum tide and is thereby easily identified from imagery and aerial photographs (Zhang et al., 2002). Remote sensing has played an essential role in shoreline extraction in several studies (Ji et al., 2009, Rokni et al., 2014, Yang et al., 2015, Li and Gong, 2016 and Sarp and Ozcelik, 2017).

For instance, it produces an instantaneous shoreline—the position of the land-sea meeting at one time (Boak and Turner, 2005)—but does not consider wind, wave, and tidal conditions at the time of image acquisition in the process (Boak and Turner, 2005). Tucker et al., (2004) state that Landsat imagery is suitable for monitoring shoreline changes because it is the only data that records land-sea conditions globally at a spatial scale of 30 m for 37 years. Apart from being available free of charge, it also has multispectral characteristics and easy acquisition. With these advantages, it creates a great opportunity for researchers to be able to map and monitor changes in natural and human phenomena that occur in coastal areas.

Many scholars have applied different methods in shoreline extraction, including single-band (Marfai et al., 2008), band ratio (Kuleli et al., 2011), supervised classification (Gautam et al., 2015), and unsupervised classification (Haibo et al., 2011). Each method has advantages and limitations in its implementation (Yang et al., 2015). In connection with shoreline dynamics, it is necessary to employ a fast and accurate method of shoreline extraction from remote sensing to enable shoreline data updating in a short time and complete shoreline data that is otherwise difficult to obtain through terrestrial and hydrographic surveys (Wicaksono and Wicaksono, 2019a). Shoreline detection uses bands sensitive to water objects, which can be determined from the characteristic spectral reflectance of water. Compared to other objects, water bodies show a weak reflection, resulting in visible wavelength (480–580 nm). At 480 nm, the reflectance is about 4–5%, but it is reduced by 2–3% at 580 nm. Because water bodies have strong absorption in the near and middle infrared bands (740–2500 nm), these wavelengths are used to distinguish water from the soil, vegetation, buildings, and other land objects (Haibo et al., 2011).

However, Liu et al., (2017) state that the biggest challenge in utilizing Landsat imagery for shoreline acquisition and monitoring is the limited spatial resolution, i.e., 30 m, meaning that the minimum shoreline change that can be detected covers an area of at least 30m x 30m. Sentinel-2A imagery, launched in 2013, has a similar wavelength to Landsat but a higher spatial resolution (European Space Agency, 2015). UAVs have now grown rapidly for use in large-scale mapping (Ramadhani et al., 2015), but routine databases are not available for some locations. The Indonesian Geospatial Information Agency (*Badan Informasi Geospasial*, BIG) creates and manages national spatial data for country development. As a subagency, Parangtritis Geomaritime Science Park (PGSP) in Bantul Regency is responsible for collecting data on coastal ecosystems in Indonesia and managing small-format aerial photographs of part of the regional coast. For this reason, the photographs are used as a reference in the accuracy assessment of the shorelines extracted from Sentinel-2A imagery through spectral transformation (Sarp and Ozcelik, 2017, Elfatma, 2017 and Kelly and Gontz, 2018).

This study investigates the capability and limitations of various spectral transformations in mapping multitemporal shoreline positions from Sentinel-2A imagery. The shoreline in Bantul Regency is 16.5 km long and is mainly composed of marine deposition coasts (Pethick, 1984); only a small part of it forms organic coasts (mangroves) and land deposition coasts around the estuary. This research restricts its analytical scope to shoreline extraction in marine deposition coasts using Sentinel-2A imagery with a 20m spatial resolution, visualized on a 1: 50,000 scale map based on Tobler's First Law of Geography (Tobler, 1987). It performs several spectral transformations: AWEIsh, AWEInsh (Feyisa et al., 2014), MNDWI (Xu, 2006), NDWI (McFeeters, 1996), B3/B11 Ratio (Winarso et al., 2009), and B11 (Kasim, 2011) on Sentinel-2A images captured in 2015 through 2020. According to the available database, one set of images with the least cloud cover represents each year of observation, and all selected imagery depicts the same season. Like Manaf et al., (2017), this study uses DSAS for shoreline validation but does not compare the accuracies of land and water classifications. It does not use generalized raster data resulting from index transformation that Kazemi et al., (2009) and Forghani et al., (2018) conducted but performs simplification on shoreline vector data. The novelty of this research is, among others, to present the accuracy of shorelines extracted from Sentinel-2A images and the adjustment steps required in the automation of shoreline extraction.

2. Study Area and Data

This research is located along the coast of Bantul Regency, the Special Region of Yogyakarta, Indonesia (Figure 1). Geomorphologically, the coast can be broadly divided into two types, fluvial-origin with relatively flat topography in the western and central parts and solutional-origin (karst) with steep cliff-shaped topography in the eastern part. In the fluvial-origin, the coast has an aquifer with large potential, shallow groundwater level and is relatively unaffected by seawater intrusion.

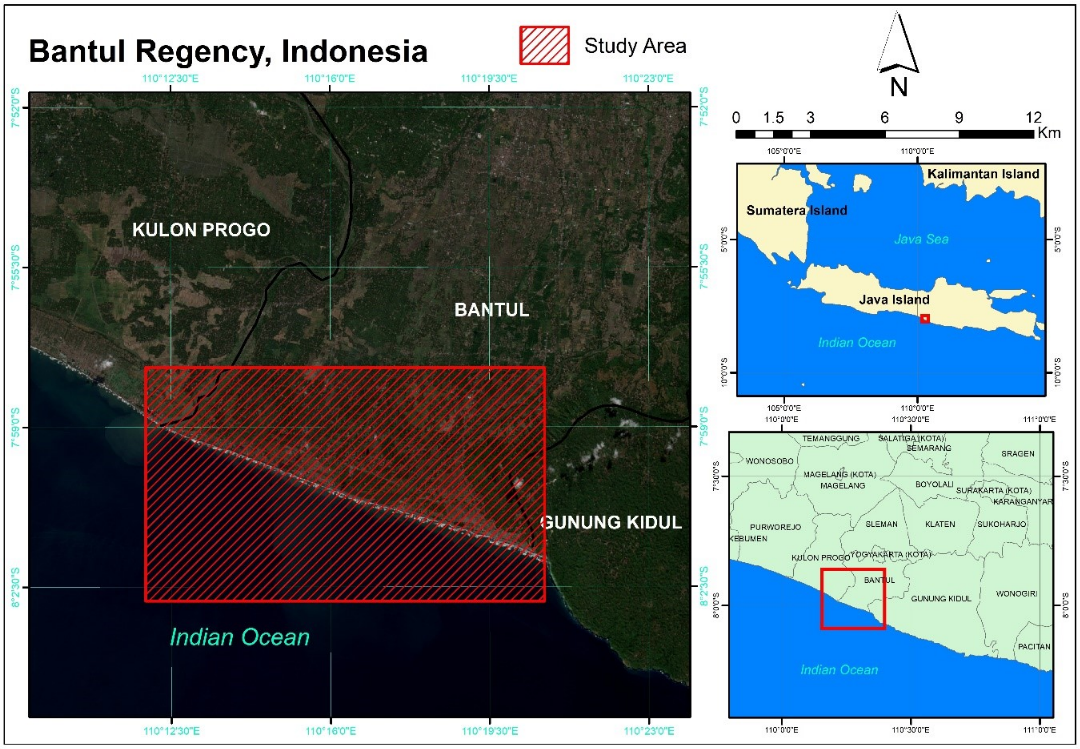

Figure 1: The study area

Loose sands that make up the area are marine deposits accumulating on the coast through combined motions of longshore currents and wave swashes. This sediment is the erosion products on Mount Merapi slopes that the Opak River carries southbound toward the Indian Ocean (Wibowo, 2001), mainly during the rainy season. When sediments reach the Indian Ocean, longshore currents immediately transport them back to the eastern coast while wave swashes move some sediments ashore. Geologically, the surface sediments of the coastal area and sandy hills are composed of alluvium (Santosa, 2016) and classified as regosols, which have little to no profile development and consist of loose materials. This soil has gray or brownish color, coarse texture, fast permeability, and relatively high sensitivity to erosion. The area has an alluvial-plain shoreline and, thus, belongs to the neutral shoreline category.

The data used are Sentinel-2A (level 1C) imagery recorded on December 26, 2015, April 24, 2016, May 19, 2017, May 14, 2018, May 29, 2019, and May 23, 2020. The use of multitemporal imagery aims to test the consistency of images and methods in extracting shorelines accurately. The image acquisition time for each year was selected by taking into account cloud cover, land-sea contrast boundaries, and data availability (Ghorai and Mahapatra, 2020). Small-format aerial photos in 2015, 2017, 2019, and 2020, as data reference, have been orthorectified with a pixel size of 0.3 m. The Sentinel-2A imagery used is only 20 m in pixel size because it has near and middle infrared bands. The 2015 image with the least cloud cover is only available for December 26, although the cloud cover is still there, while the 2017, 2019, and 2020 images are relatively clear of clouds. Tide prediction data and DEMNAS (National Digital Elevation Model) with a spatial resolution of 8.25 m obtained from the Geospatial Information Agency (www.tides.big.go.id) were used for tidal correction between the shorelines extracted from Sentinel-2A imagery and small-format aerial photographs (Kasim, 2011 and Wicaksono et al., 2018).

3. Methodology

3.1 Image Pre-Processing

Sentinel-2A level-1C products are corrected to ToA-Reflectance and, thus, require a BoA-Reflectance correction (level-2A) for use in shoreline extraction. The atmospheric correction from level 1C to 2A was carried out using the Sen2Cor method on SNAP software. The pixel values were then divided by 10,000 to obtain float values. Because only the 2019 small-format aerial photos from PGSP use ground control points (GCP), photos taken in other years were corrected geometrically by first-order polynomial image-to-image registration and GCP determination; Around 30 GCPs were distributed with the 2019 aerial photos serving as the basis. After geometric correction, the Sentinel-2A imagery for each year was corrected geometrically by first-order polynomial image-to-image registration (Danoedoro, 2012) with small-format aerial photographs serving as the basis, allowed RMSE of < 10 m, and 20 GCPs. Cloud masking was carried out per year of observation using the cloud distribution data available in the file MSK_CLDPRB_20m.jp2 when downloading the Sentinel-2A image.

3.2. Image Processing

A spectral transformation is a form of spectral sharpening that can highlight information on water bodies and distinguish them from other objects. The single-band and two-bands index threshold values were determined with the commonly used water extraction method because its calculation requires less time than other approaches (Ryu et al., 2002). Water index transformation is a band ratio method that uses two multispectral image bands and takes advantage of differences in spectral response at different land cover types (Sun et al., 2012). McFeeters (1996), Xu (2006) and Pardo-Pascual et al., (2012) prove that the water index transformation method has several advantages: ease of use and short processing time in shoreline data extraction. Some of the spectral transformation formulas used for shoreline extraction (Equations 1–6) are as follows:

$$\text{AWEInsh (non-shadow)} = 4 \times (B3 - B11) - (0{,}25 \times B8A + 2{,}75 \times B12) \quad \text{Equation 1}$$

$$\text{AWEIsh (shadow)} = B2 + 2{,}5 \times B3 - 1{,}5 \times (B8A + B11) - 0{,}25 \times B12 \quad \text{Equation 2}$$

$$\text{MNDWI} = (B3 - B11) / (B3 + B11) \quad \text{Equation 3}$$

$$\text{NDWI} = (B3 - B8A) / (B3 + B8A) \quad \text{Equation 4}$$

$$\text{Ratio Band} = B3 / B11 \quad \text{Equation 5}$$

$$\text{Single Band} = B11 \quad \text{Equation 6}$$

Where B2 = Blue Band, B3 = Green Band, B8A = NIR Band, B11 = SWIR1 Band, B12 = SWIR2 Band of Sentinel-2A Imagery. The land-sea separation was carried out by adjusting the threshold on the pixel values of the spectrally transformed image. The threshold was obtained with Otsu's image thresholding algorithm (Otsu, 1975). This separation enables automatic shoreline detection (Wicaksono et al., 2019) using the Binary Thresholding Function command on the ArcMap software, which is a specific command that separates land-sea features using the threshold values resulted from the Otsu algorithm. Pixels with a value equal to or higher than the Otsu threshold were classified as water and given the value 1. On the other hand, those classified as non-water objects were given the value 0. Water and non-water boundaries were defined as a shoreline indicator.

3.3. Shoreline Analysis

DSAS is a plugin running on the ArcMap software that calculates position difference statistics from a series of shoreline data (Kuleli, 2010, Kuleli et al., 2011, Sutikno et al., 2016 and Fuad et al., 2017). DSAS, to carry out its functions, needs a database, shoreline data, and baseline data. The baseline was used as the starting point for all DSAS transects to compute position change statistics (Himmelstoss et al., 2018). The shoreline obtained from the land-sea separation using the Otsu threshold was then smoothed out using Polynomial Approximation with Exponential Kernel (PAEK) and the maximum error tolerance of 100 m (Wicaksono et al., 2019). Reference shoreline was visually interpreted from shoreline features located at the high-water line position (HWL) on small-format aerial photographs (Boak and Turner, 2005). It was also observed in the field, which appeared as a contrast between wet and dry soils (Figure 2) and a mark left by the last high tide on the beach (Pajak and Leatherman, 2002 and Bachrodin, 2012). Any shifts between shorelines extracted from Sentinel-2A imagery and small-format aerial photograph were calculated based on tidal conditions (Table 1) and slope; then, the Sentinel-2A shoreline was adjusted using the spatial adjustment tool on ArcMap to minimize tide effects.

Sample points for the shoreline's geometric accuracy assessment were determined on the DSAS application. They were created based on the intersection of the shoreline and the transect. The transects were also made on DSAS by setting the length at 550 m and the distance between transects at 50 m, which was determined based on variations in shoreline geometry (Wicaksono and Winastuti, 2020).

Figure 2: Delineation of the High-Water Line boundary on a UAV-derived image with RGB composite

Table 1: Tidal conditions

Imagery	Acquisition Time			Tidal Condition	
	(mm-dd-yyyy)	(hh:mm:ss) GMT	(hh:mm:ss) Local	Relative Height (m)	Condition
S2A	12/26/2015	03:00:36.945	10:00:36.945	-0.046	Ebb
Aerial Imagery	02/11/2015	-	14:00:00	-0.154	Ebb
S2A	05/19/2017	02:55:49.243	09:55:49.243	-0.132	Ebb
Aerial Imagery	02/11/2017	-	14:00:00	0.959	Tide
S2A	05/29/2019	03:00:09.926664	10:00:09.926	0.164	Tide
Aerial Imagery	02/11/2019	-	14:00:00	-0.035	Ebb
S2A	05/23/2020	03:00:12.879496	10:00:12.879	-0.593	Ebb
Aerial Imagery	02/11/2020	-	14:00:00	0.953	Tide

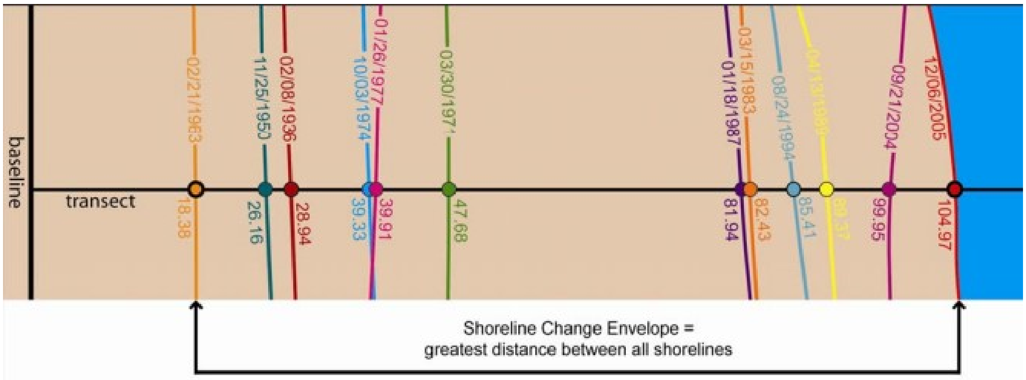

Figure 3: Illustration of SCE statistics on the DSAS application (Thieler et al., 2009)

The position difference between the spectral transformed shoreline and the reference shoreline was calculated with a DSAS statistic tool, i.e., shoreline change envelope (SCE) (Figure 3).

3.4 Geometric Accuracy Assessment

SCE produces the coordinates (X, Y) of the shoreline position as a product of the spectral transformation, the coordinates (X, Y) of the reference shoreline, and the distance between two shorelines (expressed in meters) on each transect sample made.

From this information, the horizontal RMSE can be calculated using Equation 7 (Geospatial Information Agency's Regulation Number 15 of 2014):

Horizontal RMSE =

$$\sqrt{\frac{\sum(X\ S2A - X\ UAV)^2 + (Y\ S2A - Y\ UAV)^2}{n}}$$

Equation 7

where n = sample size, X = coordinate value on the X-axis, Y = coordinate value on the Y-axis, S2A = indices-derived shoreline, UAV = reference shoreline from aerial imagery.

After the horizontal RMSE value was obtained, the horizontal geometric accuracy (CE90 value) was calculated using Equation 8, a formula by the US NMAS standard (United States National Map Accuracy Standards):

$$CE90 = 1.5175 \times RMSEr$$

Equation 8

where CE90 = Circular Error 90% is a measure of horizontal geometric accuracy (in meter) in the form of the radius of a circle indicating 90% of the error or difference between the horizontal position of a map's object and a position considered to be not actually greater than that radius, RMSEr = Horizontal Root Mean Square Error. Afterward, the geometric accuracy (in RMSE) of the shoreline data derived from spectrally transformed Sentinel-2A images was converted into horizontal accuracy (CE90) then compared with the horizontal accuracy class written in the Geospatial Information Agency's Regulation Number 6 of 2018 on Technical Guidelines for Base Map Accuracy (Table 2). The entire research flow is depicted in Figure 4.

4. Results

The pixel value of Sentinel-2A imagery before atmospheric correction is in the range of tens to thousands, but it has a range of unit values afterward. The geometric correction between aerial photographs produced an RMSE of 0.78–6.35 m, while the Sentinel-2A images that were geometrically corrected with aerial photographs had an RMSE of 6.69–8.2 m. Cloud masking using the cloud distribution data from files embedded in the Sentinel-2A imagery did not show satisfying results because, visually, some cloud cover was not cut off and potentially affected the results of further processing. Every image in the years of observation was subject to the same cloud cutting method.

Table 2. Horizontal accuracy of topographical maps (in meter)

Map Scale	Class 1	Class 2	Class 3
1:50.000	15	30	45

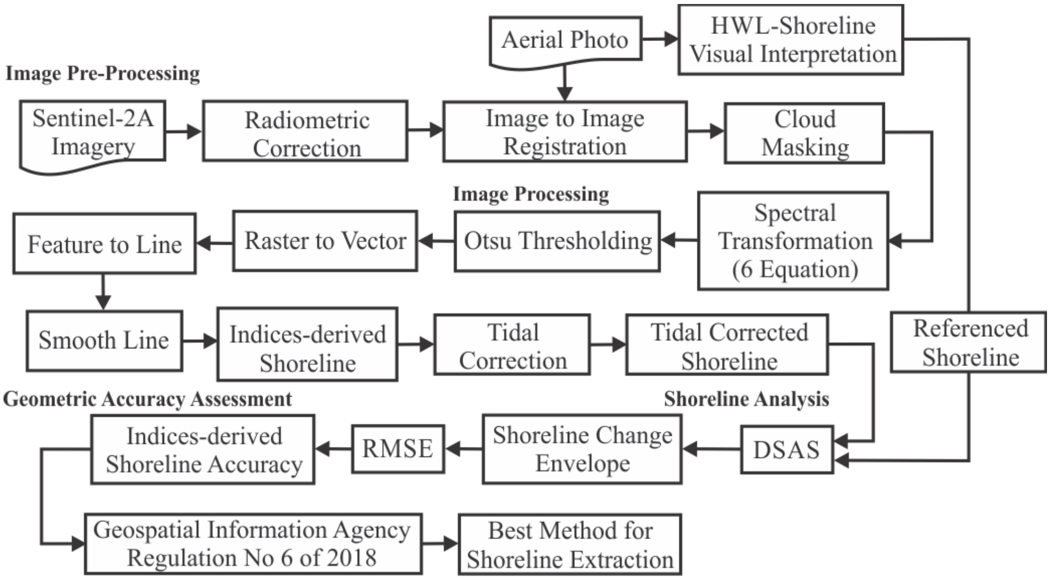

Figure 4: The research methodology flow

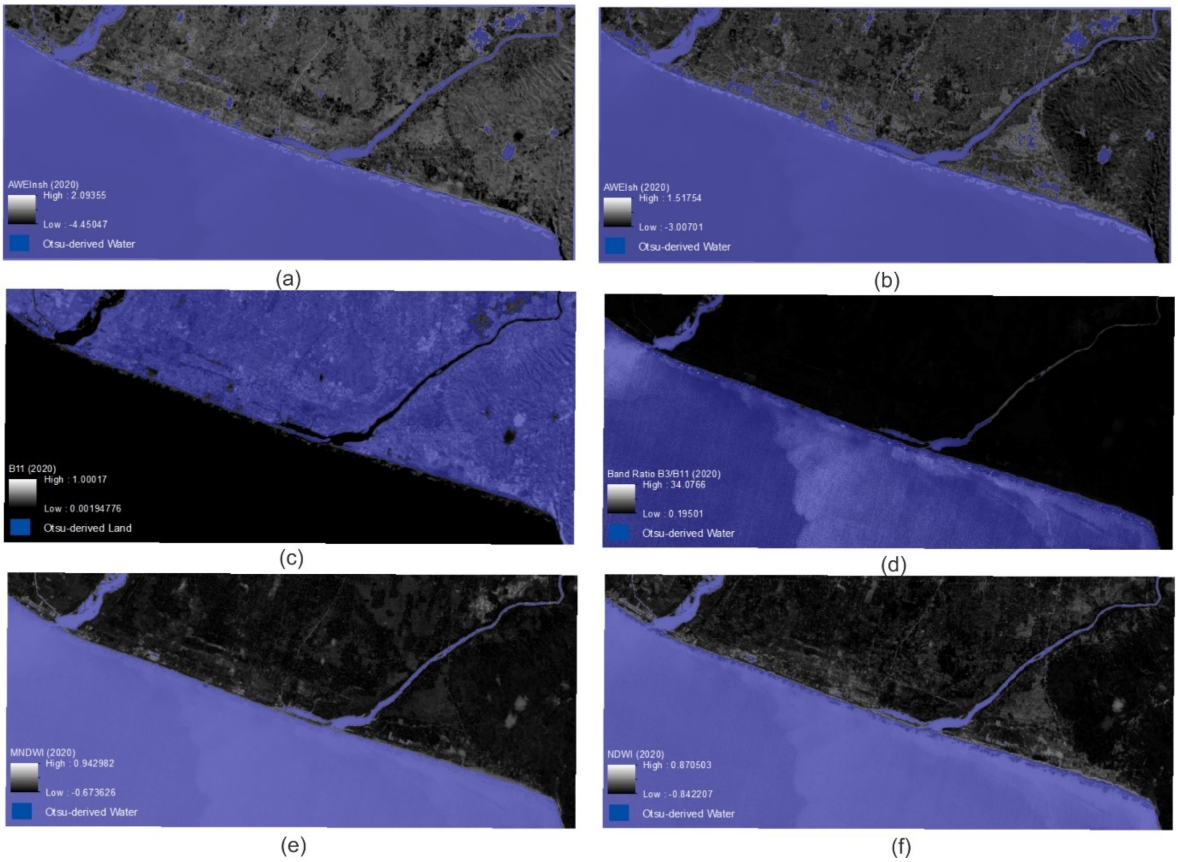

Figure 5: Land-sea separation (Otsu threshold) on spectrally transformed Sentinel-2A imagery recorded on May 23, 2020 with: (a) AWEInsh, (b) AWEIsh, (c) B11, (d) B3 / B11 Ratio, (e) MNDWI, and (f) NDWI

Table 3: The land-sea separation for each spectral transformation method using the Otsu's image thresholding algorithm

Date	Cloudy Pixel (%)	Cloud Shadow (%)	AWEInsh	AWEIsh	B11	B3/B11 Ratio	MNDWI	NDWI
12/26/2015	28	2.40	-0.34	-0.16	0.12	4.15	0.21	0.04
04/24/2016	6.15	1.49	-0.32	-0.15	0.12	1.38	0.17	-0.04
05/19/2017	3.42	1.35	-0.38	-0.24	0.1	5.14	0.17	0.01
05/14/2018	0.46	0.21	-0.32	-0.19	0.11	1.42	0.13	-0.02
05/29/2019	4.14	1.16	-0.39	-0.2	0.11	2.49	0.1	-0.07
05/23/2020	7.52	1.69	-0.37	-0.22	0.1	4.31	0.15	-0.04

After the pre-processing stage, the spectral transformation was carried out using equations 1 to 6 for each year of observation. The range of pixel values generated in each method varied, as shown in Figure 5. On relatively cloud-free images (e.g., May 23, 2020), the Otsu algorithm could separate land from the sea, and their different appearances are even visible at a glance. However, there is a mismatch in pixels located on land-sea boundaries (i.e., shorelines), especially in the foam along the shore and river estuaries. The threshold determination for land-sea separation on spectrally transformed images for each year of observation using the Otsu algorithm is presented in Table 3. The threshold values were consistently in the range of -0.3 to -0.4 for AWEInsh, -0.15 to -0.25 for AWEIsh, around 0.1 for B11, 0.1 to 0.2 for MNDWI, and -0.1 to 0.5 for NDWI. Meanwhile, the threshold values produced in the B3/B11 ratio varied greatly between 1 and 5. In other words, B11 is the easiest method to determine the Otsu threshold value, followed by MNDWI. Meanwhile, the most difficult ones are the B3/B11 ratio and NDWI because the threshold values produced for each year of observation show a wide variation.

The spectral transformation-derived shoreline and reference shoreline derived from the aerial photographs were processed on DSAS using SCE. The results showed that the distances between the spectral transformation-derived shoreline and the reference shoreline varied, as presented in Table 4. NDWI and B3/B11 ratio produced shorelines with the smallest difference from the reference shoreline (< 0.2 m), while AWEIsh produced the largest difference (> 350 m). Even so, MNDWI generated shoreline data with the smallest average variation (i.e. 27 m) and a standard deviation (i.e. 24 m). SCE was used to calculate RMSE (equation 7) and CE90 (equation 8), and the results are presented in Table 5. Referring to the Geospatial Information Agency's Regulation Number 6 of 2018, all shorelines have the horizontal accuracy of class 3 for a 1: 50,000 map scale. Based on the geometric accuracy assessment of the spectral transformation-derived shoreline presented in Table 5, for each year, MNDWI consistently gave the smallest RMSE, even though the number of observed samples in each year was different. The RMSE in question varied between 32 and 64 m (Table 6), which is 1.5–3 times larger than the pixel size of the Sentinel-2A image. The MNDWI-derived shoreline map is presented in Figure 6. The shoreline was obtained automatically from the results of digital image processing without removing shoreline data that contained errors. The 2017 to 2020 shorelines are relatively accurate because they show the actual boundaries between land and sea. Meanwhile, the 2015 and 2016 shorelines (Figures 7 and 8) contain errors because some of their segments are located on the sea due to high cloud cover on actual shorelines, namely 28% and 6%, respectively.

5. Discussion

MNDWI produces the smallest error in shorelines identification on a marine deposition coast consisting of volcanic sand beaches. Wet soil generally has high spectral reflectance at the mid-infrared region (B11) but low at the far-infrared region (B12) because of the water absorption influence.

Tabel 4: Descriptive statistics for the shoreline change envelope calculation of spectral transformation-derived shorelines

Descriptive Statistics	Date	Shoreline Change Envelope (in meter)					
		AWEInsh	AWEIsh	B11	B3/B11 Ratio	MNDWI	NDWI
Minimum	2015	0.57	5.26	5.19	0.86	0.88	0.15
	2017	0.13	1.59	0.09	0.33	0.05	0.02
	2019	0.16	3.98	0.03	0.02	1.25	0.04
	2020	0.17	17.24	0.47	0.05	0.05	0.14
Average	2015	60.25	156.14	64.95	108.81	40.46	47.47
	2017	59.18	117.55	40.80	86.06	32.78	33.65
	2019	29.43	86.17	26.40	39.33	27.07	35.85
	2020	56.54	104.13	45.72	32.21	32.23	41.04
Maximum	2015	323.23	358.84	192.50	198.74	249.71	218.03
	2017	399.79	384.64	176.90	217.74	90.77	98.92
	2019	337.11	338.94	337.11	98.58	78.60	314.61
	2020	418.38	418.38	415.15	130.45	104.54	372.83
Standard Deviation	2015	57.81	96.00	50.46	55.84	51.37	60.19
	2017	77.06	93.49	31.67	53.00	21.72	22.85
	2019	46.42	64.36	45.21	22.46	18.65	47.64
	2020	55.18	56.74	53.99	28.36	24.10	42.23

Tabel 6:The lowest RMSE of the spectral transformation-derived shorelines at a scale of 1: 50,000

Year	Best Method	RMSE (m)
2015	MNDWI	64.96
2017	MNDWI	39.3
2019	MNDWI	32.84
2020	MNDWI	40.19

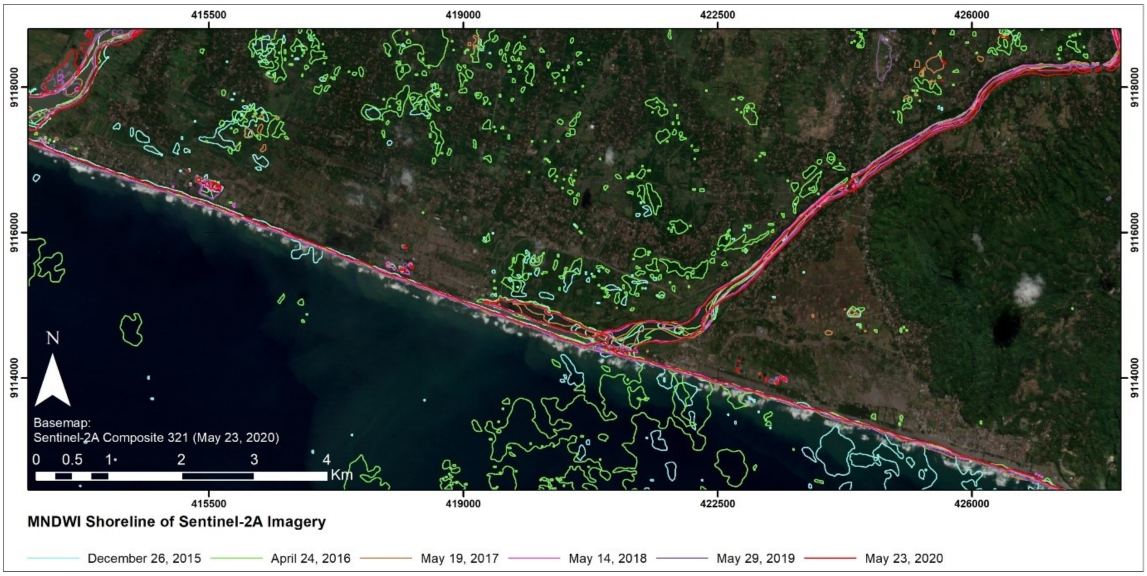

Figure 6: MNDWI-derived shorelines on Sentinel-2A imagery in 2015-2020

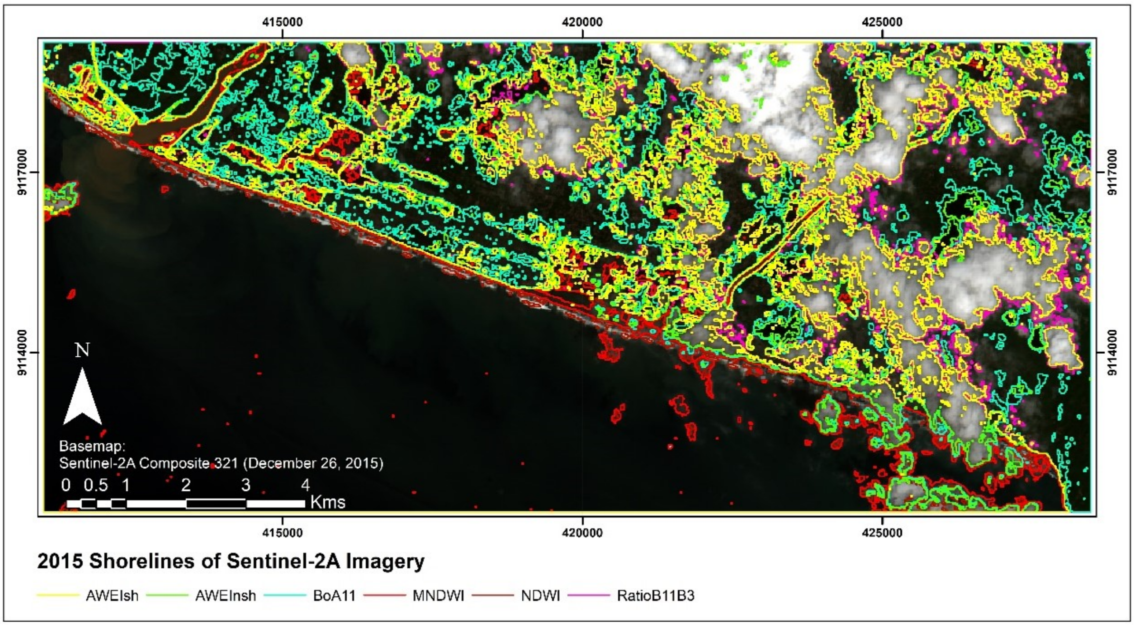

Figure 7: Indices-derived shorelines on Sentinel-2A imagery on December 26, 2015

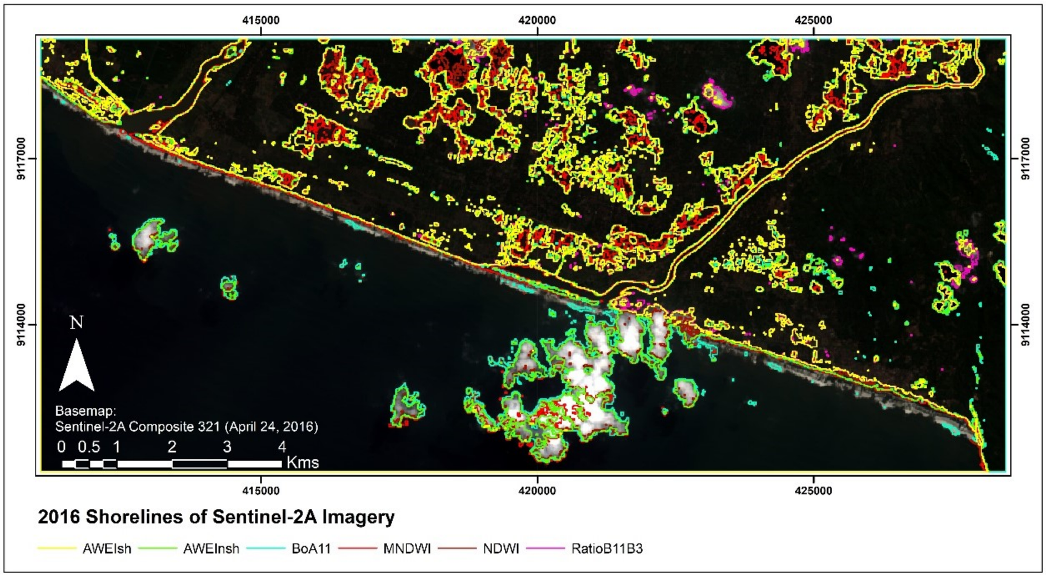

Figure 8: Indices-derived shorelines on Sentinel-2A imagery on April 24, 2016

For this reason, the pixel value of water objects in MNDWI is more positive (and that of the land object is more negative) compared to AWEI and NDWI; hence, the smallest RMSE in MNDWI shorelines, especially when the threshold was set at zero (Table 2). Moreover, based on the temporal analysis results, the MNDWI shorelines consistently have the smallest RMSE in shoreline identification for each year of observation compared to other spectral transformations (standard deviation is presented in Table 3).

The shoreline accuracy results classify MNDWI as the best shoreline identification method, and several studies have found evidence to support this assertion. Using Landsat TM, Xu (2006) and Sun et al., (2012) explain the superiority of MNDWI in extracting water bodies surrounded by non-built-up land and waters with low sediment concentrations. Wicaksono and Wicaksono (2019b) state that MNDWI provides the lowest RMSE compared to NDWI and AWEI in shoreline extraction in land deposition, marine deposition, and volcanic coasts using Landsat 8 OLI. Wicaksono and Wicaksono (2019a) further confirm that the same case is true for shoreline extraction in volcanic coasts with sandy beaches. Despite the research of Xu (2006), Sun et al. (2012), Wicaksono and Wicaksono (2019a and 2019b) use Landsat imagery as a data source, but the MNDWI transformation method still yields the best results of shoreline identification compared to other methods. However, Kasim (2011) shows different results in that the single band method, such as band 5 and B5/B2 ratio in Landsat 5 TM and Landsat 7 ETM + imagery, is highly suitable for determining land-sea boundaries in sandy coastal areas. Using Landsat TM, Feyisa et al., (2014) propose that AWEI can suppress classification disturbances from shadows and other non-water dark surfaces. However, the resulting RMSE is not smaller than the 2015 and 2016 shorelines extracted with MNDWI from images with relatively wide cloud cover.

In the shoreline data derived from spectral transformations, the land-sea separation is a crucial factor. Yang et al., (2015) suggest that the spatiotemporal variation of objects around a water body can lead to variability in the threshold; therefore, users must consider the conditions during the image recording and specific water characteristics when selecting spectral transformations. Besides, as Ji et al., (2009) observed, the presence of water, soil, and vegetation fractions in mixed pixels due to less detailed spatial resolution leads to incorrect classification because it increases threshold variability. Shorelines extracted from different locations require different threshold settings even though they share the same coastal physical typology and land cover classification. The source of errors in shoreline extraction from the imagery, as reviewed by Wicaksono et al., (2019), includes cloud cover, cloud shadow, and foam. Although the land cover in the study area is relatively homogeneous, these noises cause mixed pixels to interfere with the shoreline extraction process. The image used to identify the shoreline position in each year of observation has the minimum percentage of cloud cover for that year (Table 3).

Table 7: Shoreline uncertainties of Sentinel-2A imagery

Date (mm/dd/yyyy)	Uncertainty (in meters)			Total Uncertainty
	Geometric Accuracy RMSE	Pixel Size	Horizontal Offset of Tides	
12/26/2015	6.64	20	1.37	28.01
05/19/2017	8.20	20	13.84	42.04
05/29/2019	6.69	20	2.52	29.21
05/23/2020	5.76	20	19.61	45.37

However, the percentage is still relatively high (28% in 2015), and the cloud cover is right above the shoreline (Figures 7 and 8), thus obscuring the shorelines underneath. The high RMSE of the shoreline derived through spectral transformation (Table 5) reaches 1.5–3 times greater than the pixel size of the Sentinel-2A image (20 m). Apart from several sources of error, it is also attributed to the high uncertainty of the data sources used. Kelly and Gontz (2020) calculated the uncertainty based on geometric accuracies of data, pixel size, and horizontal offset of tides. In the current study, the uncertainty of the shoreline data sources used in Table 7 varied between 28.01 and 45.37 m. Errors in geometric correction between images have resulted in an RMSE smaller than half the pixel size, but this value has not been augmented by the bias of HWL that represents an instantaneous shoreline indicator. The 2015 image was the only one recorded during high tide (Table 1), whereas the 2017, 2019, and 2020 images were captured in different tidal conditions—the information they present is validated with aerial photograph data. Unavailable field data as a comparison creates an obstacle for this study.

This study shows that tidal correction is necessary, even in an image with a pixel size of 20 m, because the local topography in the marine deposition coast observed consists of relatively flat to gentle slopes (0–2°). The difference in the shoreline position between before and after tidal correction can reach 7.5 m. The marine deposition coast in Bantul Regency is ideal for shoreline geometric accuracy experiments because it has a low sediment concentration and relatively homogeneous land cover. However, clouds and cloud shadows create a limitation to remote sensing research of passive systems in tropical regions (Wicaksono and Wicaksono, 2019b). The wavy shoreline geometry (Retnowati et al., 2012) makes shoreline variation undetectable in Sentinel-2A imagery with a pixel size of 20 m (Wicaksono et al., 2019). This study also found that in using HWL as an instantaneous shoreline indicator in addition to the physical characteristics of the research area (Boak and Turner, 2005), it is necessary to pay attention to the tidal conditions of the images used. The horizontal offset of tides will be lower when the test data and validation data have the same tidal conditions or when the test data are recorded at high tides.

6. Conclusions

Sentinel-2A imagery with a pixel size of 20 m can be used to extract multitemporal shorelines at a scale of 1: 50,000 using several options of spectral transformation methods: single band, band ratio, and water index transformation (AWEI, MNDWI, NDWI). Based on the geometric accuracy of the shoreline—assessed with the standard issued in the Geospatial Information Agency's Regulation Number 6 of 2018, all spectral transformation methods meet the standards of class 3. Among the methods used, MNDWI produces shoreline data with the lowest RMSE (i.e., 32–64 m). This study has several limitations: (1) the small-format aerial photos were not recorded at the same as the Sentinel-2A images due to database limitations and (2) the shoreline in Bantul Regency is highly dynamic because of oceanographic and anthropogenic factors (i.e., iron sand mining), which makes the reference shoreline contain bias even after the geometric and tidal corrections.

This research investigates the ability of Sentinel-2A imagery with a spatial resolution of 20 m to extract shoreline data. Furthermore, it has more wavelength options than the one with a 10m spatial resolution, enabling the comparison of various spectral transformation methods. It is highly suggested that further research on the geometric accuracy assessment of satellite-derived shoreline to use and compares images with a spatial resolution of 10 m or higher and to perform image processing with fusion method (pan-sharpening) to increase the pixel size and, consequently, produce maps in detailed scale.

Acknowledgments

This research was funded by Universitas Gadjah Mada under the Final Project Recognition scheme in 2020. The authors would like to thank Dr. Pramaditya Wicaksono for his invaluable advice in digital image processing. Gratitude is also extended to Fajrun Wahidil Muharram, S.Si. and Yuniarsita Setyo Wulandari, S.Si., staff of the Parangtritis Geomaritime Science Park, for their help in providing aerial photographs of Parangtritis Village, Bantul Regency. Also, the authors would like to thank Yanuar Sulistyaningrum, S.Pd., M.Sc. for her assistance in research administration.

References

Bachrodin, I., 2012, Penggunaan Citra Landsat Multi-temporal untuk Kajian Perubahan Garis Pantai di Jawa. *Tesis*, (Yogyakarta: Magister Geografi, Fakultas Geografi, Universitas Gadjah Mada).

Boak, E. H. and Turner, I. L., 2005, Shoreline Definition and Detection: A Review. *Journal of Coastal Research*, Vol. 21(4), 688–703.

Congalton, R. G. and Green, K., 2008, *Assessing the Accuracy of Remotely Sensed Data: Principles and Practices*, (New York: CRC Press).

Danoedoro, P., 2012, Pengantar Penginderaan Jauh Digital, (Yogyakarta: ANDI).

Dulbahri, 1983, Aplikasi CItra Landsat skala 1:250.000 untuk Studi Perubahan Garis Pantai di Daerah Jawa Tengah dan Jawa Timur, (Yogyakarta: Fakultas Geografi Universitas Gadjah Mada).

Elfatma, O., 2017, Sistem Informasi Geografi dan Penginderaan Jauh untuk Studi Pesisir: Perubahan Garis Pantai Multi-proxy di Kepesisiran DIY dan Prediksi Garis Pantai Tahun 2026. *Tesis*, (Yogyakarta: Magister Penginderaan Jauh, Fakultas Geografi Universitas Gadjah Mada).

European Space Agency, 2015, Sentinel-2 User Handbook, Revision 2, (Paris: European Space Agency).

Feyisa, G. L., Meilby, H., Fensholt, R. and Proud, S. R., 2014, Automated Water Extraction Index: A New Technique for Surface Water Mapping Using Landsat Imagery. *Remote Sensing of Environment*, 23-35.

Forghani, A., Nadimpalli, K. and Cechet, R.P., 2018, Extracting Terrain Categories from Multi-Source Satellite Imagery. *International Journal of Geoinformatics*, Vol. 14(2),1-10.

Fuad, M. A., Saleh, R. and Handayani, M., 2017, Automatic Detection of Decadal Shoreline Change on Northern Coastal of Gresik, East Java. *Proceeding of The 5th Geoinformation Science Symposium*, (Yogyakarta: PUSPICS Fakultas Geografi Universitas Gadjah Mada), Vol. 98(1), 1-10. DOI:10.1088/1755-1315/98/1/012001.

Gautam, V. K., Gaurav, P. K. and Annadurai, M., 2015, Assessment of Surface Water Dynamicsin Bangalore Using WRI, NDWI, MNDWI, Supervised Classification and K-T Transformation. *Aquatic Procedia*, Vol. 4, 739-746.

Geospatial Information Agency, 2014, Peraturan Kepala Badan Informasi Geospasial Nomor 15 Tahun 2014 tentang Pedoman Teknis Ketelitian Peta Dasar, (Cibinong: Geospatial Information Agency).

Geospatial Information Agency, 2018, Peraturan Kepala Badan Informasi Geospasial Nomor 6 Tahun 2018 tentang Perubahan atas Peraturan Kepala Badan Informasi Geospasial Nomor 15 Tahun 2014 tentang Pedoman Teknis Ketelitian Peta Dasar, (Cibinong: Geospatial Information Agency).

Ghorai, D., and Mahapatra, M., 2020, Extracting Shoreline from Satellite Imagery for GIS Analysis. *Remote Sensing in Earth Systems Sciences*, Vol. 3, 13-22.

Girres, J. F. and Touya, G., 2010, Quality Assessment of the French Open Street Map Dataset. *Transactions in GIS*, Vol. 14(4), 435 – 459.

Haibo, Y., Zongmin, W., Hongling, Z. and Yu, G., 2011, Water Body Extraction Methods Study Based on RS and GIS. *Procedia Environmental Science*, 2619-2624.

Himmelstoss, E. A., Henderson, R. E., Kratzmann, M. G., and Farris, A. S., 2018, Digital Shoreline Analysis System (DSAS) Version 5.0 User Guide. In Open-File Report 2018-1179. (Virginia: US Geological Survey).

Ji, L., Zhang, L. and Wylie, B., 2009, Analysis of Dynamic Thresholds for The Normalized Difference Water Index. *Photogrammetric Engineering and Remote Sensing*, 1307-1317.

Kasim, F., 2011, Koreksi Pasang Surut dalam Pemetaan Perubahan Garis Pantai Menggunakan Data Inderaja dan SIG. *Jurnal Ilmiah Agrosains Tropis*, 180-188.

Kazemi, S., Lim, S. and Rizos, C., 2009, Interactive and Automated Segmentation and Generalisation of Raster Data. *International Journal of Geoinformatics*, Vol. 5(3), 65-73.

Kelly, J. T. and Gontz, A. M., 2018, Using GPS-surveyed Intertidal Zones to Determine The Validity of Shorelines Automatically Mapped by Landsat Water Indices. *International Journal of Applied Earth Observation and Geoinformation*, Vol. 65, 92-104.

Kelly, J. T. and Gontz, A. M., 2020, Rapid Assessment of Shoreline Changes Induced by Tropical Cyclone Oma Using CubeSatImagery in Southeast Queensland, Australia. *Journal of Coastal Research*, Vol. 36(1), 72-87.

Kuleli, T., 2010, Quantitative Analysis of Shoreline Changes at the Mediterranean Coast in Turkey. *Environmental Monitoring and Assessment*, Vol. 167, 387-397.

Kuleli, T., Guneroglu, A., Karsli, F. and Dihkan, M., 2011, Automatic Detection of Shoreline Change on Coastal Ramsar Wetlands on Turkey. *Ocean Engineering*, 1141-1149.

Li, W. and Gong, P., 2016, Continuous Monitoring of Coastline Dynamics in Western Florida with A 30-year Time Series of Landsat Imagery. *Remote Sensing of Environment*, Vol. 179, 196-209.

Liu, Y., Wang, X., Ling, F., Xu, S. and Wang, C., 2017, Analysis of Coastline Extraction from Landsat 8 OLI Imagery. *Water*, 1-26.

Manaf, S. A., Mustapha, N., Sulaiman, M. N., Husin, N. A. and Shafri, H. Z. M., 2017, Validation Assessment of Shoreline Extraction on Medium Resolution Satellite Image. *The 2nd International Conference on Applied Science and Technology 2017 (ICAST'17)*, 020001, 1-6.

Marfai, M. A., Almohammad, H., Dey, S., Susanto, B. and King, L., 2008, Coastal Dynamic and Shoreline Mapping: Multi-Sources Spatial Data Analysis in Semarang Indonesia. *Environmental Monitoring and Assessment*, 297-308.

McFeeters, S. K., 1996, The Use of the Normalized Difference Water Index (NDWI) in the Delineation of Open Water Features. *International Journal of Remote Sensing*, 1425-1432.

Otsu, N., 1975, A Threshold Selection Method from Gray-Level Histograms. *Automatica*, 23-27.

Pajak, M. J. and Leatherman, S., 2002, The High Water Line as Shoreline Indicator. *Journal of Coastal Research*, Vol. 18(2), 329-337.

Pardo-Pascual, J. E., Almonacid-Caballer, J., Ruiz, L. A. and Palomar-Vazquez, J., 2012, Automatic Extraction of Shoreline from Landsat TM dan ETM+ Multi-temporal Images with Subpixel Precision. *Remote Sensing of Environment*, 1-11.

Pethick, J., 1984, An Introduction to Coastal Geomorphology, (London: Edward Arnold Ltd).

Ramadhani, Y. H., Rokhmatulloh, Poniman, A. and Susanti, R., 2015, Small Island Mapping with Object Based Approach Using Unmanned Aerial Vehicle (UAV) Data: Case Study in Pramuka Island, Seribu Islands. *Majalah Ilmiah Globë,* Vol. 17(2), 125-134.

Retnowati, A., Marfai, M. A. and Sumantyo, J. T. S., 2012, Rip Currents Signatures Zone Detection on Alos Palsar Image at Parangtritis Beach, Indonesia. *Indonesian Journal of Geography*, Vol. 44(1), 12–27.

Rokni, K., Ahmad, A., Selamat, A. and Hazini, S., 2014, Water Feature Extraction and Change Detection Using Multitemporal Landsat Imagery. *Remote Sensing*, 4173-4189.

Ryu, J. H., Won, S. J. and Min, K. D., 2002, Waterline Extraction from Landsat TM Data in a Tidal Flat - A Case Study in Gomso Bay, North Dakota. *Remote Sensing of Environment*, 442-456.

Santosa, L.W., 2016, Keistimewaan Yogyakarta dari Sudut Pandang Geomorfologi, (Yogyakarta: Gadjah Mada University Press).

Sarp, G. and Ozcelik, M, 2017, Water Body Extraction and Change Detection Using Time Series: A Case Study of Lake Burdur, Turkey. *Journal of Taibah University for Science*, 381-391.

Sun, F., Sun, W., Chen, J. and Gong, P., 2012, Comparison and Improvement of Methods for Identifying Waterbodies in Remotely Sensed Imagery. *International Journal of Remote Sensing*, 6854-6875.

Sinaga, T. P. and Susiati, H., 2007, Studi Pemodelan Perubahan Garis Pantai di Sekitar Perairan Tapak PLTN Semenanjung Muria. *Jurnal Pengembangan Energi Nuklir*, 1-10.

Sutikno, S., Fatnanta, F., Kusnadi, A. and Murakami, K., 2016, Integrated Remote Sensing and GIS for Calculating Shoreline Change in Rokan Estuary. *KnE Engineering*, 1-9.

Thieler, E. R., Himmelstoss, E. A., Zichichi, J. L. and Ergul, A., 2009, Digital Shoreline Analysis System (DSAS) version 4.0 - An ArcGIS Extension for Calculating Shoreline Change, (Massachusetts: US Geological Survey).

Tobler, W., 1987, Measuring Spatial Resolution. *Land*, 12-16.

Triadmojo, B., 2008, Teknik Pantai, (Yogyakarta: Beta Offset).

Tucker, J. C., Grant, D. M. and Dykstra, J. D., 2004, NASA's Global Orthorectified Landsat Data Set. *Photogrammetric Engineering and Remote Sensing*, 313-322.

Wibowo, M., 2001, Aplikasi Sistem Informasi Geografi (SIG) untuk Penataan Kawasan Pantai (Kasus Pantai Parangtritis dan Sekitarnya). *Jurnal Teknologi Lingkungan*, Vol. 2(2), 159–167.

Wicaksono, A., Wicaksono, P., Khakhim, N., Farda, N. M. and Marfai, M. A., 2018, Tidal correction effects analysis on shoreline mapping in Jepara Regency. *Journal of Applied Geospatial Information*, Vol. 2(2),145-151.

Wicaksono, A. and Wicaksono, P., 2019a, Akurasi Geometri Garis Pantai Hasil Transformasi Indeks Air pada Berbagai Penutup Lahan di Kabupaten Jepara. *Majalah Geografi Indonesia*, Vol. 33(1), 86-94.

Wicaksono, A. and Wicaksono, P., 2019b, Geometric Accuracy Assessment for Shoreline Derived from NDWI, MNDWI, and AWEI Transformation on Various Coastal Physical Typology in Jepara Regency using Landsat 8 OLI Imagery in 2018. *Geoplanning: Journal of Geomatics and Planning*, Vol. 6(1), 55-72.

Wicaksono, A., Wicaksono, P., Khakhim, N., Farda, N. M. and Marfai, M. A., 2019, Semi-automatic shoreline extraction using water index transformation on Landsat 8 OLI imagery in Jepara Regency. *Proc. SPIE 11372*, Sixth International Symposium on LAPAN-IPB Satellite, 113721I (24 December 2019).

Wicaksono, A. and Winastuti, R., 2020, Kajian Morfodinamika Pesisir dan Kerawanan Abrasi di Kabupaten Buleleng, Provinsi Bali. *Prosiding Seminar Nasional Pengelolaan Pesisir dan Daerah Aliran Sungai ke-5*, Tangerang Selatan: 26 September 2019, 132-140.

Winarso, G., Joko, H. and Arifin, S., 2009, Kajian Penggunaan Data Inderaja untuk Pemetaan Garis Pantai (Studi Kasus Pantai Utara Jakarta). *Jurnal Penginderaan Jauh*, 65-72.

Xu, H., 2006, Modification of Normalized Difference Water Index (NDWI) to Enhance Open Water Features in Remotely Sensed Imagery. *International Journal of Remote Sensing*, 3025-3033.

Yang, Y., Liu, Y., Zhou, M., Zhang, S., Zhan, W., Sun, C., and Duan, Y., 2015, Landsat 8 OLI Image Based Terrestrial Water Extraction from Heterogeneous Backgrounds Using A Reflectance Homogenization Approach. *Remote Sensing of Environment*, 171, 14-32.

Zhang, K., Huang, W., Douglas, B.C. and Leatherman, S. P., 2002, Shoreline position variability and long-term trend analysis. *Shore and Beach*, Vol. 70(2), 31–35.